Low-energy incomplete fusion and its sensitivity to projectile structure

Kamal Kumar,[1,*] Tauseef Ahmad,[1] Sabir Ali,[1] I. A. Rizvi,[1,†] Avinash Agarwal,[2] R. Kumar,[3] K. S. Golda,[3] and A. K. Chaubey[4]

[1]*Department of Physics, Aligarh Muslim University, Aligarh (U.P.)-202 002, India*

[2]*Department of Physics, Bareilly College, Bareilly (U.P.)-243 005, India*

[3]*NP-Group, Inter University Accelerator Center, New Delhi-110 067, India*

[4]*Department of Physics, Addis Ababa University, P.O. Box 1176, Addis Ababa, Ethiopia*

(Received 28 December 2012; published 15 April 2013)

To study the heavy-ion-induced reactions, particularly complete and incomplete fusion, the excitation functions for ^{16}O+^{165}Ho interactions at energies ≈73–105 MeV have been measured using a well-established activation technique. The excitation functions have been compared with the predictions of the statistical model code PACE4. The comparison advises that the formation of xn and pxn channels is governed only via complete fusion processes. Even after correction for precursor contribution, a significant enhancement in the production of α-emitting channels may be attributed to incomplete fusion contribution. Furthermore, in order to understand incomplete fusion reactions in a more conclusive way, the incomplete fusion fraction has been analyzed with the existing data for ^{12}C and ^{20}Ne beams on the same target (^{165}Ho) where a strong projectile structure effect has been observed, which correlates incomplete fusion reaction dynamics with the α-Q value of the projectile.

DOI: 10.1103/PhysRevC.87.044608 PACS number(s): 25.70.Jj, 25.70.Gh, 25.70.Mn

I. INTRODUCTION

In recent years, the competition between incomplete fusion (ICF) and complete fusion (CF) reaction dynamics at energies in the vicinity of Coulomb barrier (CB) has been a topic of extensive discussion among experimental as well as theoretical nuclear physicists [1–6]. The ICF reactions for the first time, around five decades ago, were observed by Britt and Quinton in the bombardment of ^{197}Au and ^{209}Bi by ^{12}C, ^{14}N, and ^{16}O projectiles at energies ≈10.5 MeV/nucleon [7]. Generally CF is assumed to be the sole contributor to the total fusion cross section [8,9] near barrier energies. However, in several studies a significant fraction of ICF has been observed at these energies [10–17].

To explain the mechanism of ICF reaction dynamics, a number of theoretical models [18–24] have been proposed. Out of these, the most commonly used models to describe ICF reactions are the breakup fusion model (BUF) [18] and sum-rule models [22,24]. According to the BUF model, the projectile is speculated to break up into α clusters as it approaches the nuclear force field of the target nucleus. In the second part of this binary process, one of the fragments of the projectile is assumed to amalgamate with the target nucleus to form an incompletely fused composite system and the remaining fragment is considered to move nearly undeviated in the forward cone with almost projectile velocity. On the contrary, to explain ICF reactions, the sum-rule model utilizes a sharp cutoff approximation. The probability of CF is assumed to be unity for $\ell \leqslant \ell_{\rm crit}$ and zero in case of $\ell > \ell_{\rm crit}$ [24].

In reality, the above-proposed models qualitatively explain experimental data at energies of ≈10 MeV/nucleon, but none of these models is able to reproduce the experimental data obtained at energies as low as ≈4–7 MeV/nucleon. Further, Parker *et al.* [25] observed forward-peaked α particles in low-Z heavy-ion interactions on ^{51}V target at energies of ≈6 MeV/nucleon. Later on several studies [1–4] were carried out in this energy regime. Moreover, to understand the dependence of ICF reaction dynamics on various entrance channel parameters, several systematics [26–32] have been studied. In Ref. [26] the incomplete fusion probability is predicted to be almost proportional to the target charge (Z_T). The proposed results in Refs. [27,28] demonstrate that the input-driven angular momentum and projectile energy are also responsible for ICF contribution. Morgenstern *et al.* [29] correlated the ICF fraction with entrance channel mass asymmetry. Singh *et al.* [4] indicated that mass-asymmetry systematics may be projectile structure dependent. In addition to this, most of the recent studies [30,31] report that α-Q values of the projectile also have an impact on ICF reaction dynamics, but limited data is available on this aspect. A detailed study of CF and ICF mechanisms, including projectile structure effects with radioactive ion beams (RIBs), might be very important for understanding reactions of astrophysical interest and for the production of new nuclei near the drip lines [32]. In this regard some more detailed experiments using RIBs are required.

Hence, to strengthen this systematics and to understand ICF dependence on entrance channel parameters, excitation functions (EFs) for several evaporation residues produced in the ^{16}O+^{165}Ho system have been measured in the projectile energy range ≈73–105 MeV. Cavinato *et al.* [33] and Sharma *et al.* [34] have also studied the same projectile-target combination and measured the EFs for the production of some isotopes of Re, W, and Ta at energies of ≈69–126 MeV and ≈67–100 MeV, respectively. However, Cavinato *et al.* have limited themselves to discussing the data concerning fusion reactions only and have not made any comment about ICF, even for those channels where enhancement in α-emitting channels was observed. However, Sharma *et al.* reported ICF contribution in a few residues.

*kamalkumar1908@gmail.com

†isarrizvi@hotmail.com

 ©2013 American Physical Society

In view of the above, a better presentation of ICF contribution and its sensitivity on various entrance channel parameters has been elaborated in this work. The data set from Ref. [34] generally agrees with our work in the common energy range. In addition to this, EFs for residues ^{175}Re and ^{175}W have been measured for the first time. Moreover, the present work not only supplements the data of earlier work [33,34], but also provides a new cross-section database and presents the influence of the ICF reaction mechanism in a more conclusive way. Besides, to examine the effect of projectile structure on ICF reaction dynamics, an attempt has been employed. In this regard, to have some systematics of ICF reactions, the reanalysis of nearby projectile-target combinations [4,35–39] in light of the present data has been carried out. This comparison reveals that ICF reactions are projectile structure dependent.

II. EXPERIMENTAL DETAILS

The experiment has been carried out using the $^{16}O^{7+}$ beam at the Inter University Accelerator Center (IUAC), New Delhi, India. A target of spectroscopically pure (99.99%) self-supporting ^{165}Ho of thickness ≈1.4–1.5 mg/cm^2 and Al-catcher foils of thickness ≈ 2.0–2.15 mg/cm^2 have been prepared using the rolling technique. Al-catcher foils of sufficient thickness have been placed behind the target foil to trap the recoiling products. These foils also work as energy degraders to cover the desired energy range. The thickness of each target and catcher foil has been separately measured through weighing and by a α-transmission method, respectively.

To measure the EFs of various evaporation residues produced in the ^{16}O+^{165}Ho system, the stack has been exposed for ≈10 h, keeping in mind the half-lives of interest. The irradiation has been carried out in the General Purpose Scattering Chamber (GPSC) using the in-vacuum transfer facility. The incident beam energy on each target foil in a stack has been estimated using the SRIM code [40]. A Faraday cup installed behind the target-catcher foil assembly to measure the beam current was maintained ≈35–40 nA. The radioactivity induced in the target-catcher assembly have been measured by a precalibrated HPGe detector coupled to a CAMAC-based FREEDOM data acquisition system developed by the IUAC [41]. The nuclear spectroscopic data used in the evaluation and the measurements of cross sections have been taken from the Radioactive Isotopes Data Table of Brown and Firestone [42] and are given in Table I. A typical γ-ray spectrum for the ^{16}O + ^{165}Ho system at ≈105 MeV has been depicted in Fig. 1, where several γ peaks corresponding to different reaction products via CF and/or ICF channels are indicated. The detector has been calibrated using γ sources of known strength. The geometry-dependent efficiency of the detector has been determined using a ^{152}Eu source at various source-detector separations. Details of various factors that may cause errors and uncertainties in the cross-section measurement are given in our recent observations [17]. Attempts have been made to minimize the uncertainties due to the factors mentioned in Ref. [17]. The overall errors in the present work have been estimated to lie between 12% and 17%.

TABLE I. List of reactions with their residues and spectroscopic properties.

Residue	$T_{1/2}$	J^π	E_γ (keV)	I^γ
^{178}Re($3n$)	13.2 min	3^+	237.0	45.0
			939.1	8.9
^{177}Re($4n$)	14.0 min	$5/2^-$	197.0	8.4
^{176}Re($5n$)	5.2 min	3^+	240.0	48.0
			109.08	25.0
^{175}Re($6n$)	6.0 min	$5/2^-$	184.5	4.8
^{177}W($p3n$)	2.25 h	$1/2^-$	186.3	8.9
			115.2	51.0
			367.5	4.24
			376.8	4.6
			416.6	6.1
			426.8	13.2
^{176}W($p4n$)	2.3 h	0^+	100.2	73.01
^{175}W($p5n$)	1.81 h	$1/2^-$	166.7	9.0
			270.25	12.6
^{176}Ta(αn)	8.09 h	1^-	201.87	5.5
			1159.2	24.6
			1225.03	6.0
^{175}Ta($\alpha 2n$)	10.5 h	$7/2^+$	349.0	11.4
			125.9	5.8
			266.9	10.8
^{174}Ta($\alpha 3n$)	62.6 min	3^+	206.5	57.0
^{173}Ta($\alpha 4n$)	3.56 h	$5/2^-$	172.2	17.5
			160.4	4.9
^{166}Tm($3\alpha 3n$)	7.7 h	2^+	778.8	18.1
			785.9	9.9

III. RESULTS AND DISCUSSION

To study the ICF reaction dynamics in ^{16}O+^{165}Ho systems, the EFs for $^{178-175}$Re, $^{177-175}$W, $^{176-173}$Ta, and ^{166}Tm residues in the above-stated energy range, populated via CF and/or ICF, have been measured. The standard formulation reported in Ref. [11] has been used to determine the production cross sections of various reaction products. A residue may populate via a specific channel often emitting several γ rays of different

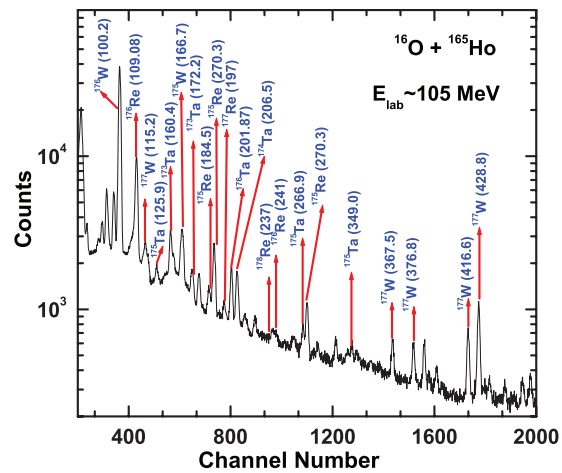

FIG. 1. (Color online) Typical spectrum of ^{16}O+^{165}Ho system using projectile beam of ≈105 MeV energy.

energies. Hence, the reported values of the cross sections for some residues are the weighted average [43] of cross sections obtained for their different γ rays.

A. Calibration of statistical model code

The experimentally measured EFs for $^{178-175}$Re evaporation residues expected to be populated via emission of xn ($x = 3$–6) from the excited composite nucleus ^{181}Re* in the interaction of ^{16}O with ^{165}Ho are shown in Fig. 2(a). The evaporated residues are identified on the basis of measured half-lives and characteristic γ-ray energies. The available data points of the previous workers [34] are also depicted in this figure, which are found consistent with the present measurements. The experimentally obtained reaction cross sections are shown in Table II. Further, in case of pxn channels, there is no α-particle emission and hence, no possibility of ICF. Therefore these channels are also expected to be populated by CF only. The experimentally deduced independent yields along with their cumulative cross sections for evaporated residues ($^{177-175}$W) populated via emission of pxn ($x = 3$–5) from the same excited composite system are plotted in Fig. 2(b). All these pxn channels are expected to be populated via both ways, namely, independently, and decay through their higher charge isobar precursors at their diagonal positions in the periodic table via β^+ decay and/or electron capture (EC). In the present case, the half-lives of the precursors are considerably smaller than those of the residues. Hence, the independent cross sections of these residues have been determined by analyzing the induced activities of their precursors using the decay analysis introduced by Cavinato *et al.* [33].

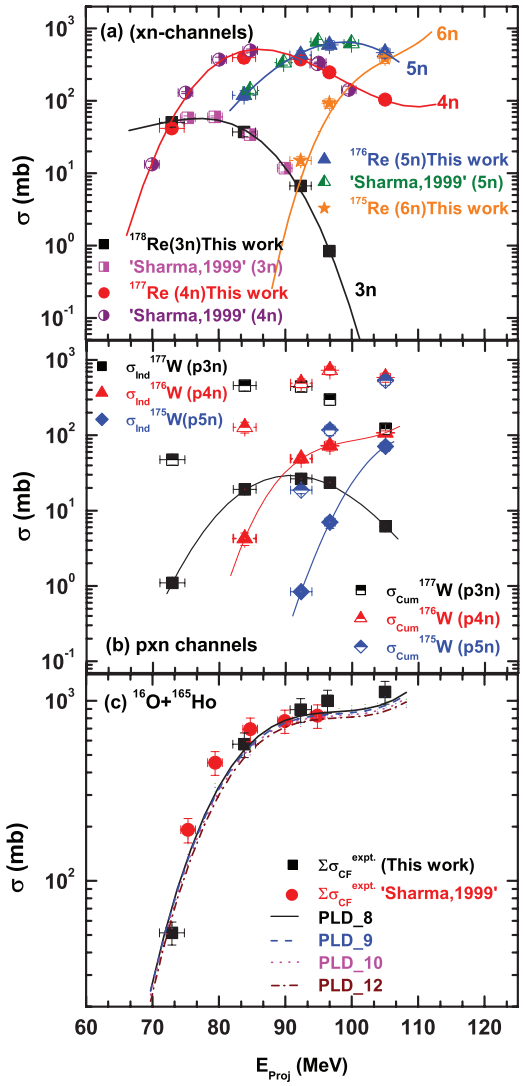

FIG. 2. (Color online) (a) Measured EFs for all xn ($x = 3$–6) channels. (b) Measured EFs for all pxn ($x = 3$–5) channels. In these figures various solid lines joining the experimental data points are just to guide the eyes. (c) Sum of all CF channels along with PACE4 calculations (for $K = 8$–10 and 12) has also been shown. The available data points of previous workers (Sharma, Ref. [34]) are also shown in this figure.

If a precursor P is formed with cross section σ_P during the irradiation and decays with half-life $t_{1/2}^P$ and a branching ratio $P_{\rm pre}$ to a daughter nucleus D, which is produced with half-life $t_{1/2}^D$, the cumulative cross section $\sigma_{\rm cum}$ in terms of independent yield $\sigma_{\rm ind}$ for the production of a daughter is given by

$$\sigma_{\rm cum} = \sigma_{\rm ind} + P_{\rm pre}\left[\frac{t_{1/2}^D}{t_{1/2}^D - t_{1/2}^P}\right]\sigma_P. \qquad (1)$$

The measured yield of $p3n$ channel is cumulative. So, by using the above formulation, the independent yield of ^{177}W can be calculated as follows:

$$\sigma_{\rm cum}(^{177}{\rm W}) = \sigma_{\rm ind}(^{177}{\rm W}) + 1.116\sigma_P(^{177}{\rm Re}). \qquad (2)$$

Similarly, the independent yields of two other pxn channels, i.e., ^{176}W and ^{175}W, may also be deduced as

$$\sigma_{\rm cum}(^{176}{\rm W}) = \sigma_{\rm ind}(^{176}{\rm W}) + 1.039\sigma_P(^{176}{\rm Re}) \qquad (3)$$

and

$$\sigma_{\rm cum}(^{175}{\rm W}) = \sigma_{\rm ind}(^{175}{\rm W}) + 1.200\sigma_P(^{175}{\rm Re}), \qquad (4)$$

where ($P_{\rm pre} = 1$) [42]. The experimentally measured independent yield of all pxn channels has also been tabulated in Table II.

To reproduce the experimental EFs via xn/pxn channels, the present analysis has been carried out in the framework of statistical model code PACE4 [44]. This code uses a Monte Carlo procedure to determine the decay sequence of an excited composite nucleus using the Hauser-Feshbach formalism [45]. The angular momentum conservation is explicitly taken into account at each step of de-excitation and the evaporation cross sections are calculated by using the Bass formula [46]. The optical model potentials of Becchetti and Greenlees [47] are used for calculating the transmission coefficients for neutrons and protons, and the optical model potential of Satchler [48] is used for α-particle emissions. In the description of γ-ray competitions, emissions of E_1, E_2, M_1, and M_2 γ rays are included and strengths for these transitions are taken from the tables of Endt [49]. The γ-decay intensities in Weisskopf units are $E_1 = 0.000\,011$, $M_1 = 0.010\,000$, $E_2 = 9.000\,000$, and $M_2 = 1.200\,000$ for the ^{16}O+^{165}Ho system. This code

TABLE II. Experimentally measured production reaction cross sections σ(mb) for all CF channels.

E_{lab} (MeV)	^{178}Re (mb)	^{177}Re (mb)	^{176}Re (mb)	^{175}Re (mb)	^{177}W (mb)	^{176}W (mb)	^{175}W (mb)
72.90 ± 1.86	50.33 ± 7.10	41.50 ± 6.00	–	–	1.10 ± 0.16	–	–
83.80 ± 1.72	36.97 ± 5.20	393.60 ± 61.60	119.36 ± 18.00	–	19.16 ± 2.87	4.26 ± 0.80	–
92.90 ± 1.60	6.67 ± 0.60	373.20 ± 53.20	428.20 ± 61.20	14.97 ± 2.10	26.50 ± 3.89	48.90 ± 5.89	0.84 ± 0.08
96.40 ± 0.80	0.84 ± 0.006	247.00 ± 33.93	588.50 ± 90.30	92.41 ± 13.60	23.45 ± 3.54	72.90 ± 11.00	7.00 ± 1.20
105.00 ± 0.78	–	103.90 ± 11.67	462.40 ± 73.20	387.50 ± 58.30	6.20 ± 0.84	107.90 ± 6.30	71.15 ± 10.30

has been modified to take into account the excitation energy dependence of the level density parameter (LDP) using the prescription of Kataria *et al.* [50]. The ground state deformation is taken as 4 $\hbar$, and the value of the fission barrier is taken as 21.89 MeV throughout the calculations.

Figure 2(c) shows a comparison of the total experimentally measured cross section of all xn/pxn channels (i.e., $\Sigma\sigma_{CF}^{expt}$) with PACE4 predictions (i.e., $\Sigma\sigma_{CF}^{Theo}$). To identify suitable LDP for the analysis of α-emitting channels, different values of the free parameter "K" (i.e., $K = 8$–10 and 12) have been tested and are shown in the same figure. As can be seen from this figure, the theoretical predictions with different input parameters are very similar and show very small change at relatively higher projectile energies. It may, however, be pointed out that a value of $K \geqslant 10$ may give rise to anomalous effects in particle multiplicity and compound nucleus temperature [51]. Although it is possible to explain all the excitation functions with different values of parameters of the code for individual channels, from the physics point of view, it is quite unreasonable. Hence, in the present work all the calculations have been carried out consistently using the same set of parameters for all the populated channels. The free parameter value of $K = 8$ has been adopted. The most important input parameters used to perform the PACE4 calculations are listed in Table III. It may, however, be pointed out that any enhancement in the EFs over the theoretical predictions may be due to a physical effect which is not included in the PACE4 code. ICF may be that effect, as suggested by several studies [1,4,12,17]. To know the extent of ICF in our case the following attempt has been made.

B. Breakup processes: Responsible for ICF contribution

The experimentally measured EFs for all αxn channels such as $^{177-x}$Ta (where $x = 1$–4) are shown in Figs. 3(a) and 3(b) and in Figs. 4(a) and 4(b), and EFs for residue ^{166}Tm via

TABLE III. The important input parameters used to perform the PACE4 calculations.

E_{lab} (MeV)	Bass fusion cross section (mb)	Fusion radius (fm)	Yrast spin ($\hbar$)	ℓ_{max} ($\hbar$)
72.90 ± 1.86	59.11	10.95	85	6
83.80 ± 1.72	529.1	10.65	95	29
92.90 ± 1.60	820.7	10.45	102	38
96.40 ± 0.80	914.8	10.35	104	41
105.00 ± 0.78	1111	10.15	110	48

($3\alpha 3n$) emission is presented in Fig. 5. Due to involvement of α particles and/or α-cluster emissions, both CF and ICF are believed to be responsible for reaction modes, namely, (i) by CF of ^{16}O followed by the formation of an excited compound nucleus (CN) ^{181}Re*, from which evaporation of neutrons and the α particles may take place, or (ii) first ^{16}O breaks into α clusters in the nuclear force field of the ^{165}Ho target such as (α+^{12}C) or (^{8}Be+^{8}Be), and then one of the fragments fuses with the target and the other fragment goes into the forward cone elastically. In this case the excited composite system is less in mass and charge as that in the case of CF, hence referred to as ICF. Therefore the reaction mechanism for the population of all observed α-emitting channels in this case is expected to be CF and/or ICF and can be represented as

(i) CF of ^{16}O, i.e.,

$$^{16}O + {}^{165}Ho \Rightarrow {}^{181}Re^* \Rightarrow {}^{177-x}Ta + \alpha + xn,$$

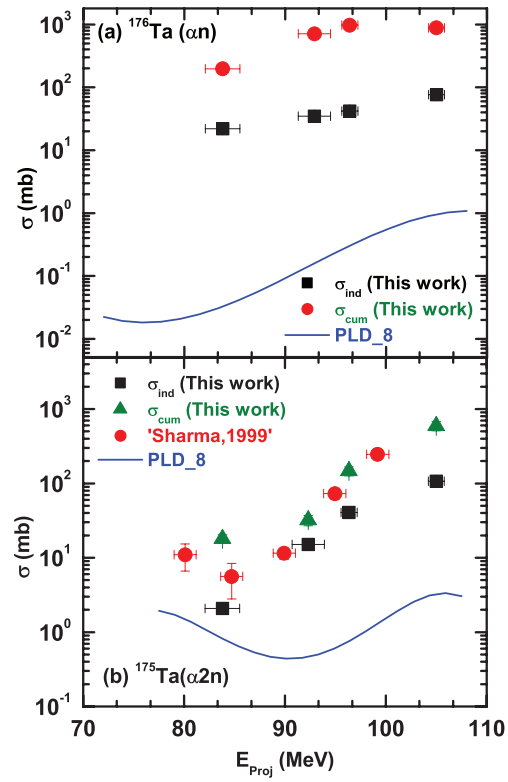

FIG. 3. (Color online) Experimentally measured EFs of ^{176}Ta (αn) and ^{175}Ta ($\alpha 2n$) along with their independent yield are shown and compared with theoretical prediction of code PACE4. The available results of previous workers (Sharma, Ref. [34]) are also shown.

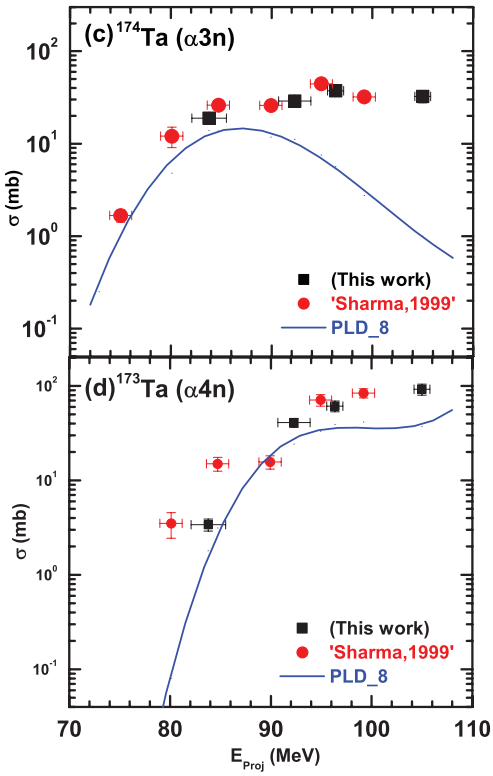

FIG. 4. (Color online) Experimentally measured EFs of ^{174}Ta ($\alpha 3n$) and ^{173}Ta ($\alpha 4n$) are shown and compared with theoretical prediction of code PACE4. The available results of previous workers (Sharma, Ref. [34]) are also shown.

(ii) ICF of ^{12}C, i.e.,

$$^{16}\mathrm{O}[^{12}C + \alpha] + {}^{165}\mathrm{Ho} \Rightarrow {}^{177}\mathrm{Ta}^* \Rightarrow {}^{177-x}\,Ta + xn$$
(α as spectator).

Moreover, the half-lives of residues ^{176}Ta and ^{175}Ta are larger than their immediate precursor (i.e., ^{176,175}W and ^{176,175}Re isotopes), so these isotopes may be produced both ways independently, as well as through decay of their higher charge isobar precursors. The cumulative cross sections of these residues are also shown in Figs. 3(a) and 3(b). Therefore in order to evaluate independent yield of these Ta isotopes, the procedure described in the previous section may be generalized to the case of more than one precursor [33]. Thus, in the case of a sequence A to B to C (here A, B, and C correspond to Re, W, and Ta, respectively), with half-lives

$$t^A_{1/2} \ll t^B_{1/2} \ll t^C_{1/2},$$

$$\sigma^C_{\mathrm{cum}} = \sigma^C_{\mathrm{ind}} + P_B\left[\frac{t^C_{1/2}}{t^C_{1/2} - t^B_{1/2}}\right]\sigma^B_{\mathrm{ind}} + P_A P_B\left[\frac{\left(t^C_{1/2}\right)^2}{\left(t^C_{1/2} - t^A_{1/2}\right)\left(t^C_{1/2} - t^B_{1/2}\right)}\right]\sigma^A_{\mathrm{ind}}, \quad (5)$$

where σ^C_{cum} represents measured cumulative yield of C, while σ^A_{ind}, σ^B_{ind}, and σ^C_{ind} represent independent yields of A, B, and C, respectively. Hence, by adopting this methodology, the independent yields of ^{176,175}Ta isotopes can be evaluated by using the following equations:

$$\sigma_{\mathrm{cum}}(^{176}\mathrm{Ta}) = \sigma_{\mathrm{ind}}(^{176}\mathrm{Ta}) + 1.398\sigma_{\mathrm{ind}}(^{176}\mathrm{W}) + 1.415\sigma_{\mathrm{ind}}(^{176}\mathrm{Re}), \quad (6)$$

$$\sigma_{\mathrm{cum}}(^{175}\mathrm{Ta}) = \sigma_{\mathrm{ind}}(^{175}\mathrm{Ta}) + 1.057\sigma_{\mathrm{ind}}(^{175}\mathrm{W}) + 1.065\sigma_{\mathrm{ind}}(^{175}\mathrm{Re}). \quad (7)$$

It may be observed from Figs. 4(a) and 4(b) that the experimentally measured cross sections are almost matching with PACE4 [44] predictions in the energy range ≈75–80 MeV (in the case of an $\alpha 3n$ channel) and ≈80–90 MeV (in case of an $\alpha 4n$ channel), respectively. However, in the higher-energy region the measured cross sections are somewhat underpredicted by PACE4 predictions. This shows that even for individual α-emitting channels, ICF takes over the regime of CF at higher excitation energies. Further, in case of reaction product ^{166}Tm ($3\alpha 3n$), the theoretical predictions of PACE4 give an almost negligible cross section and hence are not shown in Fig. 5. This indicates that the major contribution for the population of ^{166}Tm comes from an ICF process of the type

$$^{16}\mathrm{O}[\alpha + {}^{12}\mathrm{C}] \Rightarrow \alpha + {}^{165}\mathrm{Ho} \Rightarrow {}^{169}\mathrm{Tm}^* \Rightarrow {}^{166}\mathrm{Tm} + 3n$$
[^{12}C(3α) as spectator].

The measured independent yields for all αxn channels and reaction cross sections for the $3\alpha 3n$ channel are tabulated in Table IV. The experimentally measured production cross sections may be attributed to both CF and/or ICF. Although it may not be possible to obtain directly the relative contribution of ICF, an attempt has been made to extract the ICF fraction [27,28]. Hence, for a better understanding of ICF contribution in α-emitting channels, $\Sigma\sigma^{\mathrm{expt}}_{\alpha xn+3\alpha 3n}$ has been compared with that estimated by the statistical model code PACE4 $\Sigma\sigma^{PACE4}_{\alpha xn+3\alpha 3n}$ shown in Fig. 6(a). In this figure we can see that the sum of experimentally measured EFs of $\alpha xn/3\alpha 3n$ channels is significantly higher than PACE4 predictions for the same value of level density parameter (i.e., $a = A/8$ MeV^{-1}) which has been used to compare CF residues in the present work. The

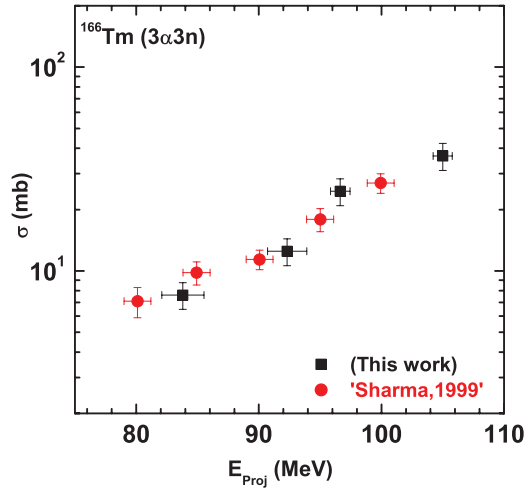

FIG. 5. (Color online) Experimentally measured EFs of ^{166}Tm ($3\alpha 3n$) are shown, while PACE4 predictions are negligibly small and hence are not shown in the graph. The available results of previous workers (Sharma, Ref. [34]) are also depicted.

TABLE IV. Experimentally measured production reaction cross-sections σ(mb) for all ICF channels.

E_{lab} (MeV)	^{176}Ta (mb)	^{175}Ta (mb)	^{174}Ta (mb)	^{173}Ta (mb)	^{166}Tm (mb)	$\Sigma\sigma_{CF}$ (mb)	$\Sigma\sigma_{ICF}$ (mb)	σ_{TF} (mb)	F_{ICF}(%)
72.9 ± 1.86	–	–	–	–	–	57.05 ± 7.1	–	57.05 ± 7.4	–
83.81 ± 1.72	22.0 ± 3.0	2.09 ± 0.3	18.91 ± 2.27	3.41 ± 0.5	7.62 ± 1.14	510.67 ± 78.3	54.03 ± 8.4	564.7 ± 84.5	9.56
92.9 ± 1.6	34.7 ± 5.4	15.16 ± 2.5	28.99 ± 4.05	40.92 ± 4.5	12.5 ± 1.88	767.12 ± 115.5	132.27 ± 19.5	899.39 ± 132.5	14.7
96.4 ± 0.8	42.07 ± 6.5	40.7 ± 6.0	37.3 ± 4.10	61.3 ± 8.00	24.59 ± 3.7	864.6 ± 121.2	205.96 ± 31.2	1070.56 ± 159.4	19.2
105 ± 0.78	76.4 ± 11.4	106.62 ± 15	32.44 ± 4.80	92.0 ± 12.30	36.67 ± 5.55	1025.4 ± 158.7	414.1 ± 53.6	1369.6 ± 202.3	30.23

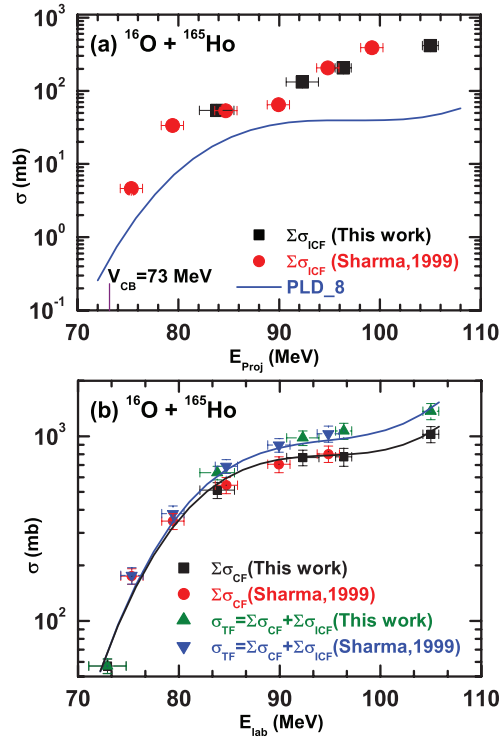

FIG. 6. (Color online) (a) Sum of all measured EFs for αxn ($x = 1 - 4$) and $3\alpha 3n$ channels plotted along with the sum of PACE4 predictions ($K = 8$) for comparison. (b) $\sigma_{TF} = \Sigma\sigma_{CF} + \Sigma\sigma_{ICF}$ is plotted with $\Sigma\sigma_{CF}$. Separation in two curves increases with energy. The available data points of previous work (Sharma, Ref. [34]) are also shown. In this figure different solid lines are just to guide the eyes.

observed enhancement in measured EFs over values predicted by PACE4 may be attributed to ICF. As can be seen from Fig. 6(a), the ICF contribution starts in the vicinity of CB (≈3% above the V_{CB}). The contribution of ICF in the production of α-emitting channels has been deduced as $\Sigma\sigma_{ICF} = \Sigma\sigma_{expt} - \Sigma\sigma_{PACE4}$. In order to see how much ICF contributes to the total reaction cross section ($\sigma_{TF} = \Sigma\sigma_{CF} + \Sigma\sigma_{ICF}$), the sum of cross sections of all CF channels ($\Sigma\sigma_{CF}$) and σ_{TF} as a function of incident projectile energy is plotted in Fig. 6(b). As can be seen from this figure, the increasing separation between $\Sigma\sigma_{CF}$ and σ_{TF} with incident projectile energy indicates the energy dependence of ICF.

To study the dependence of ICF on different entrance channel parameters the percentage ICF fraction (% F_{ICF}) has been deduced for the ^{16}O+^{165}Ho system. The F_{ICF} is a measure of relative strength of ICF to the total fusion and is defined as $F_{ICF}(\%) = \frac{\Sigma\sigma_{ICF}}{\sigma_{TF}} \times 100$. The calculated percentage ICF fraction has been listed in Table IV.

C. Mass asymmetry systematics: Sensitive to projectile structure

In this sequence, as inferred by Morgenstern *et al.* [29], the ICF reaction dynamics is governed by the relative velocity ($v_{relative}$) of the projectile and mass asymmetry [$M_a = A_T/(A_T + A_P)$] of interacting partners. An attempt

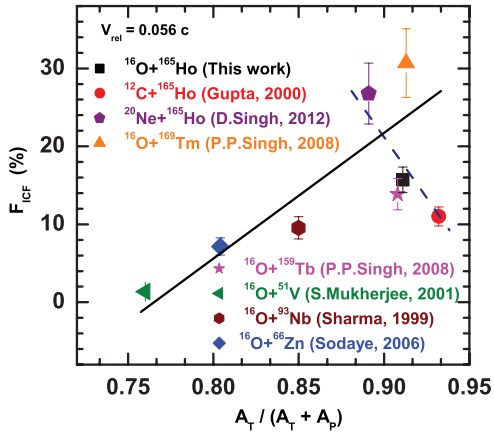

FIG. 7. (Color online) Deduced percentage ICF fraction ($F_{\rm ICF}$) for the present system (^{16}O+^{165}Ho) as a function of mass symmetry at $v_{\rm rel} = 0.056$c along with values available in literature (Singh [4], Gupta [35], Singh [36], Mukherjee [37], Sharma [38], and Sodaye [39]). Solid line is drawn just to guide the eyes.

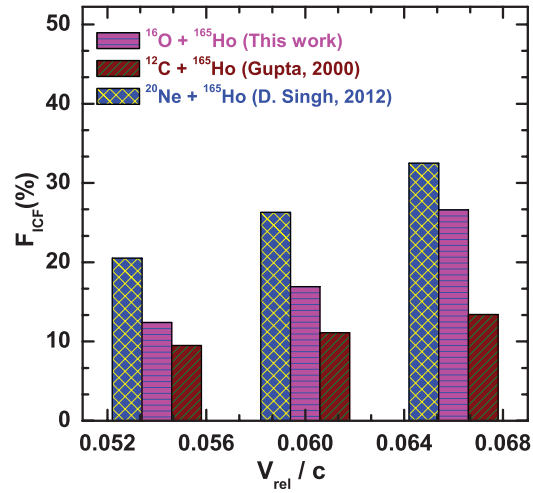

FIG. 8. (Color online) Deduced percentage ICF fraction ($F_{\rm ICF}$) as a function of α-Q value for systems ^{12}C+^{165}Ho (Gupta [35]), ^{16}O+^{165}Ho (present work), and ^{20}Ne+^{165}Ho (Singh [36]) at different relative velocities. The α-Q value of each projectile is also exhibited.

has also been made to investigate the effect of mass-asymmetry systematics. In Fig. 7, the value of $F_{\rm ICF}$ of the present system ^{16}O+^{165}Ho is plotted along with those obtained in Refs. [4,35–39] at a constant relative velocity (i.e., $v_{\rm rel} = 0.056$c). As can be seen from this figure, in general, the data points suggest more ICF probability for more mass asymmetric than symmetric systems, which is in accordance with Morgenstern *et al.* [29]. However, the values of $F_{\rm ICF}$ for the systems [35,36] are not following the same trend.

The above conflict in Fig. 7 may be due to the projectile structure effect along with the mass asymmetry of interacting partners, which can be understood in terms of α-Q value of the projectile, as suggested in previous reports [30,31]. As a consequence, Babu *et al.* [30] and Yadav *et al.* [31] have found that for low α-Q value projectiles, the obtained $F_{\rm ICF}$ is high at the same normalized projectile energies. In their work Yadav *et al.* used systems ^{12}C+^{159}Tb, ^{16}O+^{159}Tb, and ^{13}C+^{159}Tb for comparison, while Babu *et al.* used ^{12}C+^{181}Ta and ^{13}C+^{181}Ta. Hence, to check the validity of this aspect for the α-clustered projectiles, the present work has been undertaken. In order to assess this unusual behavior of mass asymmetry systematics, the $F_{\rm ICF}$ for the two systems [35,36] along with the present work at different relative velocities has been plotted in Fig. 8. The calculated α-Q values for projectile fragmentation are

$$^{20}\mathrm{Ne} \Rightarrow \alpha + {}^{16}\mathrm{O}; \quad Q_\alpha = -4.73\ \mathrm{MeV},$$
$$^{16}\mathrm{O} \Rightarrow \alpha + {}^{12}\mathrm{C}; \quad Q_\alpha = -7.16\ \mathrm{MeV},$$
$$^{12}\mathrm{C} \Rightarrow \alpha + {}^{8}\mathrm{Be}; \quad Q_\alpha = -7.37\ \mathrm{MeV},$$

making ^{20}Ne and ^{16}O more unstable in this regard than ^{12}C in the nuclear field of the same target (^{165}Ho). The obtained trend is found consistent with the previous studies [30,31]. Hence, the α-Q value may be liable for this unusual trend in Fig. 7. Hence, it may be worth mentioning that along with mass asymmetry of interacting partners, the projectile structure (which predominantly depends on the α-Q value of the projectile) also plays an important role in ICF reaction dynamics. Furthermore, to have a more clear picture about the projectile structure effect on ICF, some extended studies are needed in different mass regions.

IV. CONCLUSIONS

To observe the influence of the entrance channel parameters on ICF reaction dynamics, an attempt has been made to measure EFs for the production of 12 radio nuclides, $^{178-175}$Re(xn, $x = 3$–6), $^{177-175}$W(pxn, $x = 3$–5), $^{176-173}$Ta(αxn, $x = 1$–4), and ^{166}Tm($3\alpha 3n$) in the energy range $\approx$73–105 MeV. The present analysis has been carried out within the framework of the statistical model code PACE4. EFs for all CF channels are found consistent with the PACE4 predictions. During the analysis, it has been found that all the pxn, αn, and $\alpha 2n$ channels have contributions from their higher-charge isobar precursors, which has been reduced to get the independent yield of the respective evaporation residues. In the present work it has been found that ICF reactions are influenced by projectile structure along with projectile energy and mass asymmetry of the interacting partners. It seems that the α-Q value is responsible for this projectile structure effect. However, these aspects can be strengthened by carrying out studies with more target-projectile combinations.

ACKNOWLEDGMENTS

The authors thank the IUAC, New Delhi, India, for providing all the facilities to carry out the experiment and analysis. We are also thankful to the Chairman, Department of Physics, AMU, Aligarh, India, for providing all necessary facilities. K.K. thanks the UGC, New Delhi, India, for providing financial support in the form of JRF (NET). We are also thankful to Dr. Abhishek Yadav for important discussions related to this article. S.A. also extends his gratitude towards UGC, New Delhi, India, for financial assistance in the form of SRF (MANF).

[1] F. K. Amanuel, B. Zelalem, A. K. Chaubey, A. Agarwal, I. A. Rizvi, A. Maheshwari, and T. Ahmed, Phys. Rev. C **84**, 024614 (2011).

[2] A. Yadav, V. R. Sharma, P. P. Singh, D. P. Singh, M. K. Sharma, U. Gupta, R. Kumar, B. P. Singh, R. Prasad, and R. K. Bhowmik, Phys. Rev. C **85**, 034614 (2012).

[3] D. P. Singh, Unnati, P. P. Singh, A. Yadav, M. K. Sharma, B. P. Singh, K. S. Golda, R. Kumar, A. K. Sinha, and R. Prasad, Phys. Rev. C **80**, 014601 (2009).

[4] P. P. Singh, B. P. Singh, M. K. Sharma, Unnati, D. P. Singh, R. Prasad, R. Kumar, and K. S. Golda, Phys. Rev. C **77**, 014607 (2008).

[5] A. Diaz-Torres, D. J. Hinde, J. A. Tostevin, M. Dasgupta, and L. R. Gasques, Phys. Rev. Lett. **98**, 152701 (2007).

[6] A. Diaz-Torres and I. J. Thompson, Phys. Rev. C **65**, 024606 (2002).

[7] H. C. Britt and A. R. Quinton, Phys. Rev. **124**, 877 (1961).

[8] M. Dasgupta, P. R. S. Gomes, D. J. Hinde, S. B. Moraes, R. M. Anjos, A. C. Berriman, R. D. Butt, N. Carlin, J. Lubian, C. R. Morton, J. O. Newton, and A. S. de Toledo, Phys. Rev. C **70**, 024606 (2004).

[9] L. F. Canto, R. Donangelo, L. M. deMatos, M. S. Hussein, and P. Lotti, Phys. Rev. C **58**, 1107 (1998).

[10] P. R. S. Gomes, I. Padron, E. Crema, O. A. Capurro, J. O. Fernández Niello, A. Arazi, G. V. Marti, J. Lubian, M. Trotta, A. J. Pacheco, J. E. Testoni, M. D. Rodriguez, M. E. Ortega, L. C. Chamon, R. M. Anjos, R. Veiga, M. Dasgupta, D. J. Hinde, and K. Hagino, Phys. Rev. C **73**, 064606 (2006); P. R. S. Gomes, I. Padron, M. D. Rodríguez, G. V. Marti, R. M. Anjos, J. Lubian, R. Veiga, R. Liguori Neto, E. Crema, N. Added, L. C. Chamon, J. O. Fernández Niello, O. A. Capurro, A. J. Pacheco, J. E. Testoni, D. Abriola, A. Arazi, M. Ramírez, and M. S. Hussein, Phys. Lett. B **601**, 20 (2004).

[11] F. K. Amanuel, B. Zelalem, A. K. Chaubey, A. Agarwal, I. A. Rizvi, A. Maheshwari, and T. Ahmad, Eur. Phys. J. A **47**, 156 (2011).

[12] M. Dasgupta, D. J. Hinde, A. Mukherjee, and J. O. Newton, Nucl. Phys. A **787**, 144 (2007).

[13] P. P. Singh, B. P. Singh, M. K. Sharma, U. Gupta, R. Kumar, D. Singh, R. P. Singh, S. Murlithar, M. A. Ansari, R. Prasad, and R. K. Bhowmik, Phys. Lett. B **671**, 20 (2009); P. P. Singh, A. Yadav, D. P. Singh, U. Gupta, M. K. Sharma, R. Kumar, D. Singh, R. P. Singh, S. Muralithar, M. A. Ansari, B. P. Singh, R. Prasad, and R. K. Bhowmik, Phys. Rev. C **80**, 064603 (2009).

[14] S. Chakrabarty, B. S. Tomar, A. Goswami, G. K. Gubbi, S. B. Manohar, A. Sharma, B. B. kumar, S. Mukherjee, Nucl. Phys. A **678**, 355 (2000).

[15] A. Yadav, V. R. Sharma, P. P. Singh, M. K. Sharma, D. P. Singh, Unnati, R. Kumar, B. P. Singh, R. Prasad, and R. K. Bhowmik, EPJ Web of Conferences **17**, 16019 (2011).

[16] P. P. Singh, M. K. Sharma, Unnati, D. P. Singh, R. Kumar, K. S. Golda, B. P. Singh, and R. Prasad, Eur. Phys. J. A **34**, 29 (2007); P. P. Singh, A. Yadav, D. P. Singh, U. Gupta, M. K. Sharma, K. S. Golda, R. Kumar, R. P. Singh, S. Muralithar, B. P. Singh, R. K. Bhowmik, and R. Prasad, Eur. Phys. J. Web of Conferences **2**, 10004 (2010).

[17] A. Agarwal, S. Dutt, A. Sharma, I. A. Rizvi, K. Kumar, S. Ali, T. Ahmad, R. Kumar, and A. K. Chaubey, Eur. Phys. J. Web of Conferences **38**, 17001 (2012).

[18] T. Udagawa and T. Tamura, Phys. Rev. Lett. **45**, 1311 (1980).

[19] J. P. Bondrof, Nucl. Phys. A **333**, 285 (1980).

[20] V. I. Zagrebaev, Ann. Phys. (NY) **197**, 33 (1990).

[21] R. Weiner and M. Weström, Nucl. Phys. A **286**, 282 (1977).

[22] J. Wilczynski, K. Siwek-Wilczynska, J. Van Driel, S. Gonggrijp, D. C. J. M. Hageman, R. V. F. Janssens, J. Łukasiak, R. H. Siemssen, and S. Y. Van Der Werf, Nucl. Phys. A **373**, 109 (1982).

[23] J. R. Wu and I. Y. Lee, Phys. Rev. Lett. **45**, 8 (1980).

[24] K. Siwek-Wilczynska, E.H. duMarchievanVoorthuysen, J. vanPopta, R. H. Siemssen, and J. Wilczynski, Phys. Rev. Lett. **42**, 1599 (1979).

[25] D. J. Parker, J. J. Hogan, and J. Asher, Phys. Rev. C **39**, 2256 (1989).

[26] D. J. Hinde, M. Dasgupta, B. R. Fulton, C. R. Morton, R. J. Wooliscroft, A. C. Berriman, and K. Hagino, Phys. Rev. Lett. **89**, 272701 (2002).

[27] T. Ahmad, I. A. Rizvi, A. Agarwal, R. Kumar, K. S. Golda, and A. K. Chaubey, Int. J. Mod. Phys. E **20**, 645 (2011).

[28] A. Agarwal, I. A. Rizvi, R. Kumar, B. K. Yogi, and A. K. Chaubey, Int. J. Mod. Phys. E **17**, 393 (2008).

[29] H. Morgenstern, W. Bohne, W. Galster, K. Grabisch, and A. Kyanowski, Phys. Rev. Lett. **52**, 1104 (1984).

[30] K. S. Babu, R. Tripathi, K. Sudarshan, B. D. Srivastva, A. Goswami, and B. S. Tomar, J. Phys. G: Nucl. Part. Phys. **29**, 1011 (2003).

[31] A. Yadav, V. R. Sharma, P. P. Singh, R. Kumar, D. P. Singh, Unnati, M. K. Sharma, B. P. Singh, and R. Prasad, Phys. Rev. C **86**, 014603 (2012).

[32] A. Mukherjee, S. Roy, M. K. Pradhan, M. S. Sarkar, P. Basu, B. Dasmahapatra, T. Bhattacharya, S. Bhattacharya, S. K. Basu, A. Chatterjee, V. Tripathi, and S. Kailas, Phys. Lett. B **636**, 91 (2006).

[33] M. Cavinato, E. Fabrici, E. Gadioli, E. Gadioli Erba, P. Vergani, M. Crippa, G. Colombo, I. Redaelli, and M. Ripamonti, Phys. Rev C **52**, 2577 (1995).

[34] A. Sharma, B. B. Kumar, S. Mukherjee, S. Chakrabarty, B. S. Tomar, A. Goswami, G. K. Gubbi, S. B. Manohar, A. K. Sinha, and S. K. Datta, Pramana J. Phys. **54**, 355 (1999).

[35] S. Gupta, B. P. Singh, M. M. Musthafa, H. D. Bhardwaj, and R. Prasad, Phys. Rev. C **61**, 064613 (2000).

[36] D. Singh, Rahbar Ali, M. Afzal Ansari, B. S. Tomar, M. H. Rashid, R. Guin, and S. K. Das, Nucl. Phys. A **879**, 107 (2012).

[37] S. Mukherjee, A. Sharma, S. Sodaye, B. S. Tomar, A. Goswami, and S. B. Manohar, Eur. Phys. J. A **12**, 199 (2001).

[38] A. Sharma, B. B. Kumar, S. Mukherjee, S. Chakrabarty, B. S. Tomar, A. Goswami, and S. B. Manohar, J. Phys. G **25**, 2289 (1999).

[39] S. Sodaye, B. S. Tomar, and A. Goswami, Pramana J. Phys. **66**, 985 (2006).

[40] The Stopping and Range of Ions in Matter (SRIM) code: [http://www.srim.org/SRIM/SRIMLEGL.htm].

[41] FREEDOM, Data Acquisition and Analysis System Designed to Support the Accelerator Based Experiments at the Inter University Accelerator Center (IUAC), New Delhi, India.

[42] E. Browne and R. B. Firestone, *Table of Radioactive Isotopes* (Wiley, New York, 1986).

[43] S. F. Mughabghab, M. Divadeenam, and N. E. Holden, *Neutron Cross-Sections* (Academic Press, New York, 1981), Vol. 1, Part A, p. 89.

[44] A. Gavron, Phys. Rev. C **21**, 230 (1980).

[45] H. Feshbach and V. F. Weisskope, Phys. Rev. **76**, 1550 (1949); H. Feshbach, C. E. Porter, and V. F. Weisskopf, *ibid.* **96**, 448 (1954).
[46] R. Bass, Nucl. Phys. A **231**, 45 (1974).
[47] F. D. Becchetti and G. W. Greenlees, Phys. Rev. **182**, 1190 (1969).
[48] G. R. Satchler, Nucl. Phys. **70**, 177 (1965).
[49] P. M. Endt, At. Data Nucl. Data Tables **26**, 47 (1981).
[50] S. K. Kataria, V. S. Ramamurthy, and S. S. Kapoor, Phys. Rev. C **18**, 549 (1978).
[51] J. P. Lestone, Phys. Rev. C **53**, 2014 (1996).